Applied Thermal Engineering 166 (2020) 114686

Contents lists available at ScienceDirect

Applied Thermal Engineering

journal homepage: www.elsevier.com/locate/apthermeng

Development and thermal performance of a vapor chamber with multi-artery reentrant microchannels for high-power LED

Liang Chen[a], Daxiang Deng[b,*], Qingsong Huang[a], Xinhai Xu[b], Yingxi Xie[c]

[a] Department of Mechanical & Electrical Engineering, Xiamen University, Xiamen 361005, China
[b] School of Mechanical Engineering and Automation, Harbin Institute of Technology, Shenzhen, Shenzhen 518055, China
[c] Guangdong Key Laboratory of Precision Equipment and Manufacturing Technique, South China University of Technology, Guangzhou 510641, China

HIGHLIGHTS

- Vapor chamber (VC) with multi-artery reentrant microchannels was developed.
- VC was integrated with a high-power LED module for efficient heat dissipation.
- The VC reduced substrate surface temperature of LED module for 7–27%.
- The VC reduced thermal resistance for 19–48% compared to copper plate.

ARTICLE INFO

Keywords:
High-power LED
Thermal management
Vapor chamber
Multi-artery reentrant microchannels

ABSTRACT

This study developed a vapor chamber (VC) with radial multi-artery reentrant microchannels for thermal management of high-power light emitting diodes (LEDs). It featured Ω-shaped reentrant microchannels inside porous wicks to provide separated flow passages for vapor and liquid flow. It was integrated with a high-power LED module for fast heat dissipation and efficient thermal management. Experiments were systematically conducted to evaluate thermal performance of the VC for a wide range of input power of LEDs, air flow rates and inclination angles of LED module. The VC was compared to a copper plate heat sink in the same operation conditions. Results show that compared to the copper plate, the VC presented a faster temperature rise, and was earlier to reach equilibrium state. The VC reduced the substrate surface temperature of LED module for 7–27%, and introduced a reduction in the thermal resistance for 19–48%, indicating that the VC enhanced cooling capacity remarkably and yield a notable favorable performance for the heat dissipations of LEDs. The thermal performance of the VC was significantly dependent on the input power of LEDs and air flow rates, whereas the inclination angle of LED module showed negligible effects on thermal performance.

1. Introduction

Light-emitting diodes (LEDs), as the fourth generation of light sources, have been extensively utilized in various lighting fields, such as street lamps, automobile headlamps, projectors and backlights of television (TV) [1,2]. LEDs feature many promising merits, i.e., long lifespan, low cost, high luminous efficiency and energy efficiency, and so on [1,3]. Nevertheless, thermal management of LEDs has become a critical issue for their application, as only approximately 20% of the supplied energy for LED is transformed into optical output power, whereas the rest is converted into wasted heat [4]. The accumulation of waste heat leads to the dominant luminescence wavelength drift, the decline of optical efficiency, as well as the degradation lifetime of the phosphor [5]. As a result, effective heat dissipations should be implemented for LEDs in urgent demand.

At present, there have been some thermal management methods for high-power LEDs such as fin heat sink [6], heat pipe [7], microchannel cooler [8], microjet array cooling [9]. Among them, fin heat sinks and heat pipes are two main methods for heat dissipations of LEDs due to their higher reliability and lower cost. The fin heat sink is restricted by its low heat transfer coefficient and large physical size, which hinders its wide application in the high-power LEDs. Heat pipes can transfer large amount of heat very quickly via evaporation and condensation of a working fluid, and maintain uniform temperature distribution owing to the inherent phase change heat transfer mechanism. They are commonly of a cylindrical shape or a flat one, i.e., flat heat pipe or vapor

* Corresponding author.
E-mail address: dengdaxiang@hit.edu.cn (D. Deng).

https://doi.org/10.1016/j.applthermaleng.2019.114686
Received 16 September 2019; Received in revised form 9 November 2019; Accepted 15 November 2019
Available online 17 November 2019
1359-4311/

chamber (VC) [10,11]. Unlike the cylindrical heat pipes, the vapor chamber is able to dissipate multiple heat spots due to its large and flat condensation area. Besides, it features great uniform temperature distribution due to its short path between the evaporator and condenser. Therefore, many attentions have been paid to the vapor chambers for the thermal management of LEDs [12–15]. Huang et al. [12] employed a vapor chamber as the heat spreader for high-power LEDs. Compared to copper and aluminum substrates, the vapor chamber reduced the spreading resistance for 34% and 56%, respectively. It also reduced the temperature differences for 4 °C and 6 °C, respectively. Wang et al. [13] developed a vapor chamber-based plate for heat dissipations of 30 W high-power LEDs. It reduced the temperature for above 10 °C compared to the LED aluminum based-plate, and its maximum effective thermal conductivity reached to be 965 W/m °C at 187.5 W/cm^2. Yang et al. [14] developed a polymer (FR4) vapor chamber for LEDs. The vapor chamber consists of a 1 mm thick copper frame, which is sandwiched between top and bottom sheets of FR4 polymer. It enhanced the heat conduction through the wall of the polymer, and reduced the thermal resistance of the substrate by 57%. Tang et al. [15] proposed an integrated heat sink with vapor chamber for the thermal management of high-power LEDs. The wicks of the vapor chamber were micro-milled parallel and orthogonal microgrooves. The results showed that the junction temperature and total thermal resistance of the vapor chamber was 13.04 °C and 16.5% lower than that of conventional heat sink, respectively. The temperature field of the vapor chamber was more uniform than the conventional heat sink.

The wick structure is the core component of a vapor chamber. It provides capillary pressure for driving the two-phase circulation, and also serves as flow paths for the permeation and recirculation of working liquid. The start-up and thermal performance of vapor chambers thus rely significantly on the wick structures. Sintered powder and grooved wicks are two common wick structures in the vapor chambers [16,17]. Large capillary pressure and excellent evaporation heat transfer performance can be provided by the sintered power wick, but its small permeability and large flow resistance of the porous structures hinders its efficient recirculation of working liquid. On the other side, the grooved wick features high permeability, whereas it provides relatively small capillary pressure. In order to balance the capillary pressure and permeability, composite wicks have been developed in vapor chambers, such as sintered powder-mesh [18], groove-mesh [19–21], and sintered powder-groove [22–27] composite wicks. Composite wicks with fine metal powders sintered onto layers of coarse pore copper meshes were developed by Franchi and Huang [18]. Enhanced heat transfer performance over homogeneous wicks was obtained. Hsieh et al. [20] proposed a vapor chambers with a groove-mesh hybrid wick for cooling LED lighting module, and superior thermal performance was achieved at inclined angles. Besides, Oshman et al. [21] fabricated a hybrid wick heat spreader with woven mesh bonded atop rectangular microgrooves. This heat spreader was found to be able to operate efficiently at adverse gravitational and dynamic acceleration situations. Tang et al. [23,25] and Deng et al. [24] developed a composite wick by covering sintered copper powder on micro V-grooves. Experimental results showed that the sintered powder-grooved composite wicks enhanced both the permeability and capillary performance compared to sintered wicks, and also provided much larger capillary pressure than grooved wicks. Subsequent heat transfer performance tests by Li et al. [26] and Jiang et al. [27] demonstrated its excellent heat transfer performance of the vapor chamber with sintered powder-grooved composite wicks.

Besides of the above reported composite wicks, sintered wick with radial multi-artery channels has been also found to be a good choice for vapor chambers. The sintered wicks provided excellent evaporation heat transfer performance and large capillary pressure. Radial multi-artery channels inside the sintered wicks provide flow passages for the circulated liquid flow to return to the center of the evaporator with low hydraulic resistance. In addition, the separation of the liquid and vapor flow can be maintained by the radial multi-artery channels to reduce the viscous force in the chamber. Therefore, enhanced thermal performance can be expected for the vapor chambers. A multi-artery vapor chamber with sintered wicks was developed by Hwang et al. [28]. The sintered wicks were of a set of rectangular channels, which serves as the lateral converging arteries for liquid flow. Very large global dryout limit of 580 W/cm^2 can be achieved by the continuous liquid supply by the lateral liquid arteries. Ju et al. [29] developed a planar vapor chamber with hybrid evaporator wicks, which consisted of vertical columnar arteries, non-uniform converging lateral arteries with rectangular channels, and biporous powder structures. The vapor chamber was able to dissipate 1500 W from a 4 cm^2 heating area. Deng et al. [30] designed a series of composite porous vapor chambers (CPVCs) with uniform rectangular radial grooves in the sintered wick of the evaporator. They were able to operate efficiently to high heat fluxes of 280 W/cm^2 without notable performance degradation.

From the above literature review, it can be noted that sintered wick with radial multi-artery channels is ideal for vapor chambers. The radial multi-artery channels reported are commonly rectangular channels. In order to enhance heat transfer performance further, vapor chambers with radial multi-artery reentrant microchannels may be a good choice. As a matter of fact, the reentrant microchannels supply as a vapor trap during nucleate boiling, and increase nucleation sites considerably [31]. Moreover, the reentrant microchannels featured large cavities inside and small slots outside, which is favorable for the separation of vapor and liquid flow and reduction of shear force for the liquid-vapor counterflow inside the two-phase flow in heat pipe. They have been recognized to be an efficient heat transfer enhancement method in cylindrical heat pipes and boiling systems [32,33]. Nevertheless, to the best knowledge of the authors', the vapor chambers with radial multi-artery reentrant microchannels are scarcely reported. To this aim, we in this study developed a novel vapor chamber with radial multi-artery reentrant microchannels in porous wicks. The developed vapor chambers were integrated with a high power LED module for fast heat dissipations and efficient thermal management. By the comparison of a copper plate, the thermal performance of the LED module with the vapor chamber was systematically evaluated in different input power of LED module, air flow rates and inclination angles.

2. Design and fabrication of vapor chamber

The designed vapor chamber with radial multi-artery reentrant microchannels is shown in Fig. 1. It consists of an evaporator and condenser plate, evaporator and condenser wicks. The vapor chamber has an outer dimension of 60 mm in diameter and about 3 mm in total in thickness. The bottom evaporator and top condenser plates are made of a 0.5 mm thick pure copper plate. The condenser and evaporator wicks are sintered onto the inner surface of the top and bottom plates directly. They are of the same spherical copper powder with a particle size of 50–75 μm. The condenser wick is of a 0.5 mm thick copper powder layer. For the evaporator wick, the total thickness of the porous layer is 1.6 mm. There is a circular cavity with the size of Φ15 × 1.1 mm, which supplies as the evaporation area and also the converging area for the storage of working liquid. Four radial fan-shaped grooves with rectangular cross-section are uniformly distributed around the circular cavity to form the main vapor flow passages. Between two radial fan-shaped grooves, there are three Ω-shaped reentrant microchannels inside the porous layer. They feature large circular cavities inside, and narrow slot upside. The geometric dimensions are shown in the enlarged view of Fig. 1. The porous powder layer of the evaporator wick are in intimate contact with the porous layer in the condenser, providing better support for the condenser and strengthen the structure of the vapor chambers remarkably. Therefore, the common copper columns inside the vapor chamber [14–16] can be eliminated.

The fabrication process of the vapor chamber is as follows: Firstly,

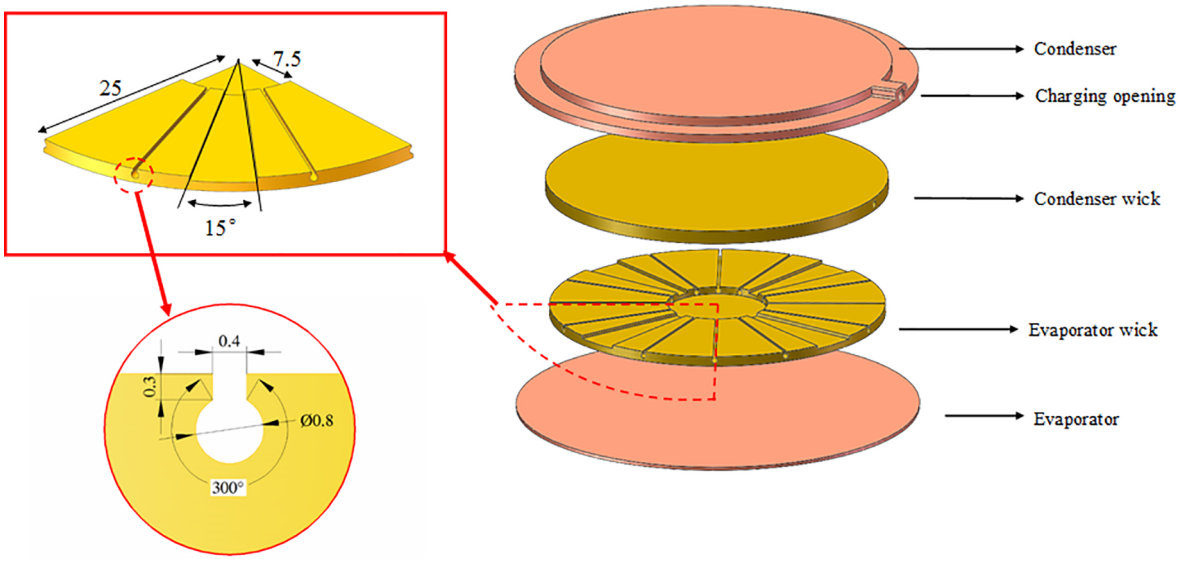

Fig. 1. Structure of vapor chamber with radial multi-artery reentrant microchannels. The unit inside is mm.

the top condenser and bottom evaporator plates are manufactured on pure copper plates by precision milling. The charging opening is formed by drilling. Then two graphite dies with designed structures are used to prepare the evaporator porous wick with four radial fan-shaped grooves and the condenser porous wick with sintered copper powder layer. During the preparation of porous wicks, copper powders are filled into the graphite dies and compacted by vibration. Then the filled dies are fixed with the copper plates. Since graphite and copper are not bonded together during high-temperature sintering, the sintered copper powder layer can be smoothly separated from the graphite dies. The wick structures and copper plates are sintered together in a furnace in a reducing atmosphere at a temperature of 950 °C for 60 min. After sintering, radial multi-artery reentrant microchannels are processed in the porous wick of the evaporator. Ω-shaped reentrant microchannels are formed inside the porous layer of evaporator. Thereafter, the top and bottom plates are welded together. A copper charging tube with a diameter of 1 mm is used as a liquid filling port and a vacuum port. The vapor chamber is evacuated at about 7 Pa and then charged with ethanol (anhydrous ethanol, A.R., 99.5%) as the working fluid. Ethanol is common working liquid for copper heat pipes or vapor chambers [30,34,35]. It features low saturation temperature or boiling point, which is ideal for rapid start-up and two-phase circulation of the vapor chamber. The filling ratio is set to be 40%. After filling, the end of the copper tubes are flatted and welded. The vapor chamber with radial multi-artery reentrant microchannels is thus obtained. Hot pressing and cold pressing are also performed to ensure the surface flatness of the vapor chamber. Fig. 2 shows the picture of the vapor chamber.

Fig. 3 shows the picture and microscopic images of the vapor chamber and its multi-artery reentrant microchannels. The Ω-shaped reentrant microchannels are formed inside the porous layer of the evaporator, which provides good flow passages for the separation of vapor and liquid flow. Numerous micro-pores formed in the sintered powder porous layer. This increases heat transfer area considerably, and also provide many nucleation sites for the boiling process during the two-phase flow circulation in the vapor chamber. Besides, the porous power layer provides excellent capillary pressure to drive the condensed liquid to return to the evaporator.

3. Experiment methods

3.1. Experiment setup

In this study, a series of 30 CREE LED lighting source (each of 5 W) are integrated with the prepared vapor chamber by a metal core printed circuit board method [36], as shown in Fig. 4(a). An insulation layer is firstly prepared on the evaporator surface of the vapor chamber. Then a circuit layer is prepared on the insulation layer. After that, the LED lighting sources are mounted on the circuit surface directly in arrays. The LED lighting sources are then bonded with vapor chamber by reflow soldering. Instead of setting a layer of thermal conductive silicone

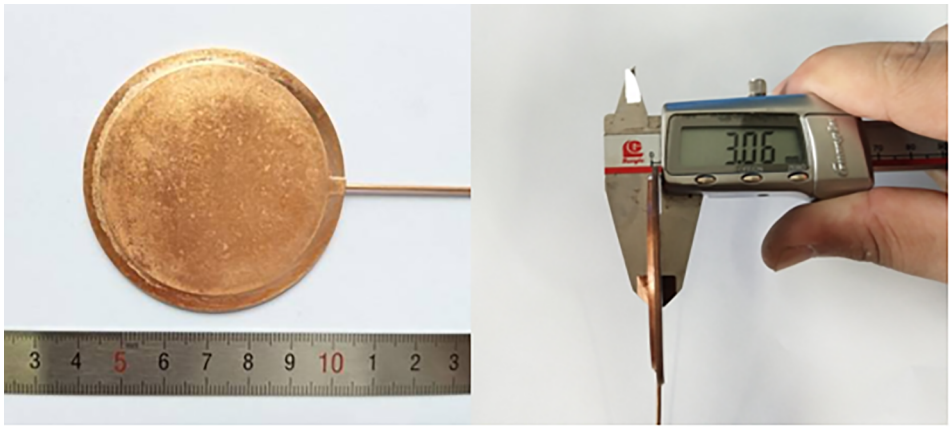

Fig. 2. Picture of the fabricated vapor chamber.

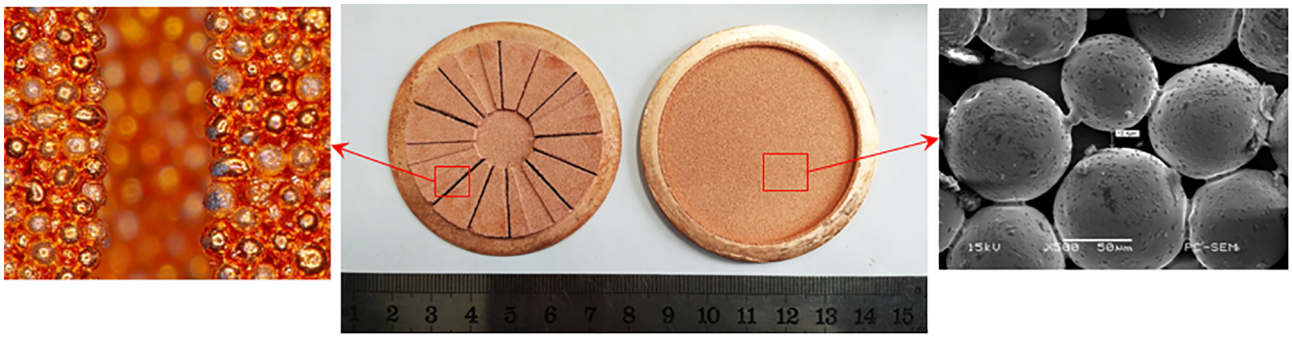

Fig. 3. Picture and microstructure of the wicks in the vapor chamber. The SEM and 3D Laser Scanning Confocal Microscope (LSM) images are shown inside.

rubber in previous studies [15,37], the contact thermal resistance between the LED and vapor chamber can be reduced remarkably by soldering. On the other side, a LED module integrated with pure copper plate is also prepared in the same way, as shown in Fig. 4(b). The size of the copper plate is same to the vapor chamber.

A series of comparative experiments are then conducted with vapor chamber and copper plate to evaluate the thermal performance.

The experimental setup is shown in Fig. 5(a). It consists of a platform which can rotate from 0 to 180°, a DC power supply, an Agilent34970A data acquisition system, and a test section with LED module. The test section consists of the LED module with vapor chamber or copper plate, a heat sink and a fan for cooling. The upper surface of condenser of vapor chamber or copper plate is attached to the bottom of heat sink, between which thermal grease with a thermal conductivity of 5 W/mK is set to minimize the thermal contact resistance. The heat sink is insulated in the periphery by setting three PEEK plates, and the heat loss can be thought to be negligible. The inclination angle of the test section is changed through 0° (horizontal position) to 90° (vertical position) by the protractor, as shown in Fig. 5(b).

The distribution of thermocouples is shown in Fig. 6. Four K-type thermocouples (T10-T13) are attached on the substrate surface of LED module to measure the evaporator surface temperature of the vapor chamber. Nine K-type thermocouples (T1-T9) are attached on the condenser surface of vapor chamber to measure the condenser surface temperature. The thermocouples distributions of the LED module with copper plate are all the same to those of vapor chambers. In the experiment, the system was placed at a thermostatic room and the ambient temperature was maintained to be 25 °C. The data was collected when the electricity was powered on, and each test lasted for 1 h to ensure that the system operated in a steady state. Those data was then synchronized to a computer at 1s intervals.

3.2. Data reduction

The heat transfer performance of vapor chamber or vapor chamber (VC) is usually evaluated by thermal resistance. It can be determined as follows:

$$R_{vc} = \frac{T_e - T_c}{Q} \tag{1}$$

where T_e is the average temperature of the evaporator surface, which can be obtained by the average of four thermocouples measurement attached on the substrate surface of LED module,

$$T_e = \frac{1}{4}\sum_{i=10}^{13} T_i \tag{2}$$

T_c is the average temperature of the condenser surface, which can be obtained as follows,

$$T_c = \frac{1}{9}\sum_{i=1}^{9} T_i \tag{3}$$

Q is the heat input to the vapor chamber by the LED module, which is approximated the power load of LEDs multiplied by 0.85 [6,37]. Therefore, the thermal resistance of vapor chamber can be calculated to be

$$R_{vc} = \frac{T_e - T_c}{UI * 0.85} \tag{4}$$

where U and I is the input voltage and current. The thermal resistance of copper plate can be calculated in the same way.

Uncertainties in individual temperature measurements are ± 0.3 °C for the accuracy of K-type thermocouples. The power provided by the DC power supply yields an uncertainty of 1%. From a standard error analysis method [38], the uncertainty of the thermal resistances can be

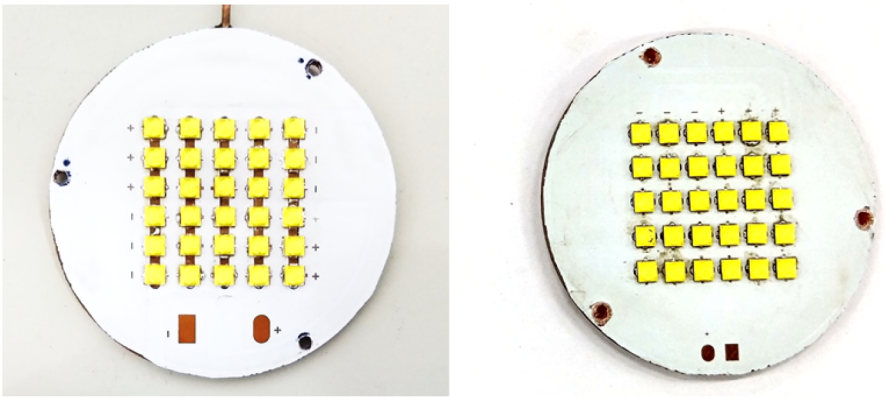

Fig. 4. Picture of LED module: (a) LED module with vapor chamber, (b) LED module with copper plate.

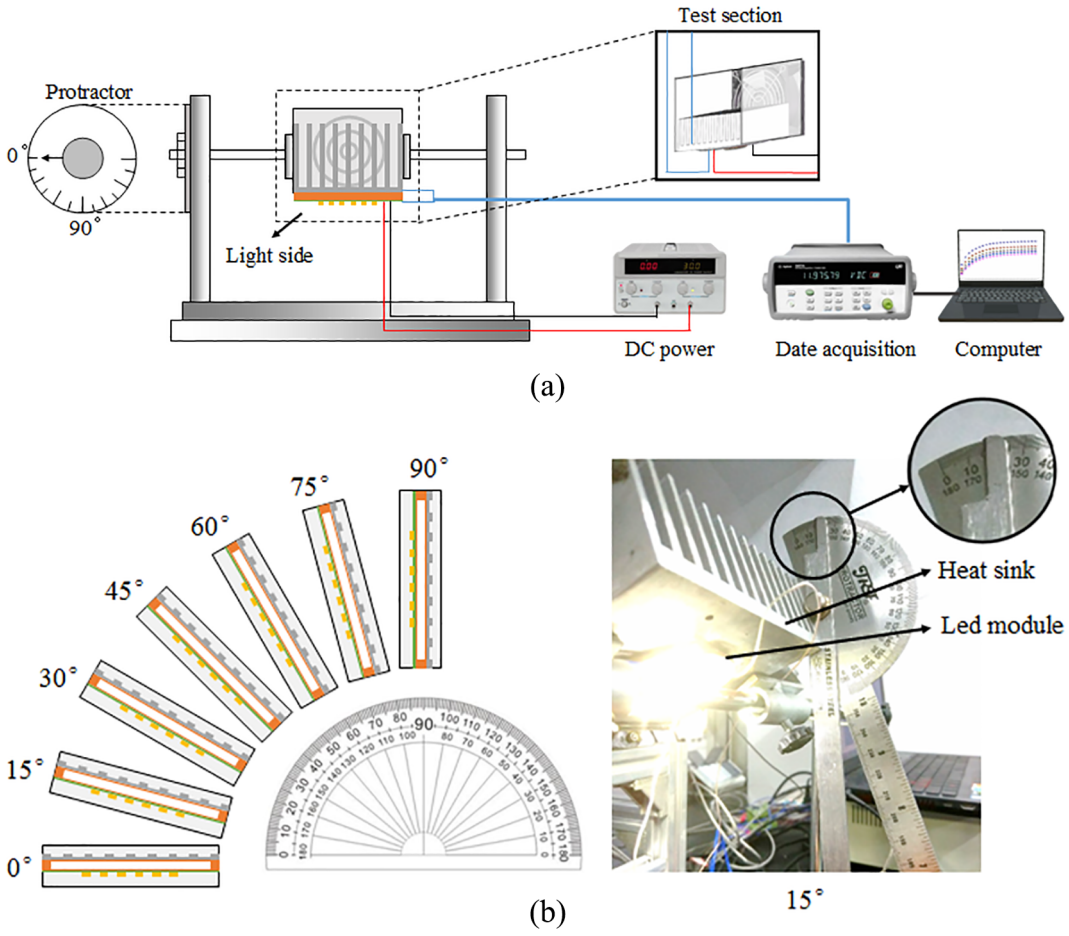

Fig. 5. Schematic of the experimental system: (a) test system, (b) LED module with different inclination angles.

estimated to be within 2.1%. The calculation process of the uncertainties of thermal resistance is as follows:

$$\delta T_e = \left\{\sum_{i=1}^{4}\left(\frac{1}{4}\delta T_{ei}\right)^2\right\}^{1/2} = \left\{\sum_{i=1}^{4}\left(\frac{T_{ei}}{4}\frac{\delta T_{ei}}{T_{ei}}\right)^2\right\}^{1/2} \quad (5)$$

$$\delta T_c = \left\{\sum_{i=1}^{9}\left(\frac{1}{9}\delta T_{ci}\right)^2\right\}^{1/2} = \left\{\sum_{i=1}^{9}\left(\frac{T_{ci}}{9}\frac{\delta T_{ci}}{T_{ci}}\right)^2\right\}^{1/2} \quad (6)$$

$$\frac{\delta R}{R} = \sqrt{\left(\frac{\delta T_e}{T_e}\right)^2 + \left(\frac{\delta T_c}{T_c}\right)^2 + \left(\frac{\delta Q}{Q}\right)^2} \quad (7)$$

4. Result and discussion

4.1. Startup characteristics

Fig. 7 illustrates transient temperature curves of LED modules with vapor chamber and copper plate at an input power of 78 W. The cooling air flow rate of the fan was 6 m/s. The start-up and running process of the vapor chamber can be roughly divided into the following three stages: (a) rising temperature stage, (b) start-up stage and (c) equilibrium state. In the rising temperature stage, the heat was mainly conducted from the LED chips to the back of the LED, and then transfer to the evaporator surface of vapor chamber. The evaporator surface

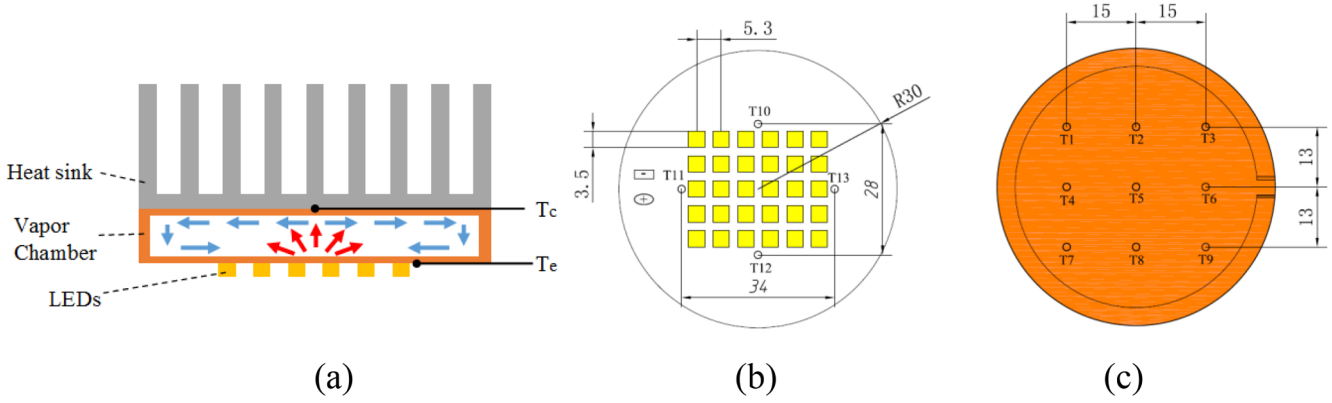

Fig. 6. Thermocouples distributions: (a) Schematic of thermocouple location on vapor chamber; (b) Thermocouples distribution on the evaporator surface; (c) Thermocouples distribution on the condenser surface.

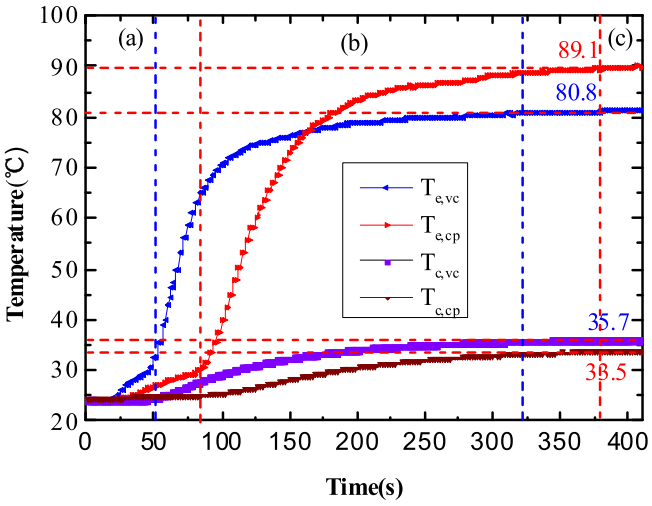

Fig. 7. Transient temperature of both vapor chamber and copper plate with the input power of 78 W of LED module.

temperature of vapor chamber ($T_{e,vc}$) began to rise. It can be noted that $T_{e,vc}$ increased faster than the surface temperature of copper plate ($T_{e,cp}$) in the initial stage, as the majority of heat from the LED chips accumulated in the evaporator of VC, and the phase change in vapor chamber was not started. On the other hand, for the copper plate, the heat can be conducted through the copper plate from the substrate surface of LED module to the bottom surface directly, and dissipated by the heat sink. After that, in the start-up stage, part of working fluid in the vapor chamber evaporated, and phase change heat transfer of working fluid began to be initiated in vapor chambers. The condenser surface temperature of vapor chamber began to increase. For the copper plate, the heat can only be dissipated through the copper material, whose thermal conductivity is much lower than the vapor chamber. This leads to higher temperature rising rate in this stage. When the heat dissipated to the environment by the heat sink was equal to the heat generated by the LED chips, the equilibrium state tended to be reached, and the surface temperatures tended to be stabilized. The successive circulation of evaporation and condensation inside the vapor chamber maintained rapid heat transfer and dissipation by the heat sink.

It can be noted from Fig. 7 that shows the evaporator surface temperature of vapor chamber ($T_{e,vc}$) in equilibrium state was 80.8 °C, much smaller than the $T_{e,cp}$ (89.1 °C) of copper plate. This result indicates that VC can reduce substrate surface temperature of LED module considerably, and showed a great superiority for thermal management of LED module. Besides, the time that it took to reach the equilibrium state of vapor chamber was much shorter than that of the copper plate, i.e., it took about 320 s for the vapor chamber when the condenser temperature was stable, whereas it took 380 s for the copper plate to the equilibrium state. Therefore, the equilibrium state can be reached earlier for vapor chamber. From Fig. 7, it can be also noted that the condenser temperature of vapor chamber was very low, just about 10 °C higher than the ambient temperature. A somewhat large temperature difference occurred from the evaporator to condenser. Such behavior has been also reported in previous works [34,39,40]. Possible reason for the above may be that the heat flux on condenser surface was dissipated quickly by the installed heat sink and cooling fan, thus the condenser temperature was maintained to be low. On the other hand, the heat flux was applied to evaporator surface continuously by the high power LEDs, which induced a large evaporator surface temperature. Besides, as the sintered porous layers in both condenser and evaporator sections featured smaller thermal conductivities than the solid copper materials, the thermal resistance induced by both sintered wick layers of evaporator and condenser and vapor flow inside the vapor chamber may also induce a remarkable temperature reduction from the evaporator to condenser.

4.2. Thermal performance

4.2.1. Thermal performance at different input power of LED module

Fig. 8(a) shows the substrate surface temperature of LED module, and Fig. 8 (b) shows the thermal resistances of vapor chamber (R_{vc}) and copper plate (R_{cp}) at different input power of LEDs. The air flow rate was 6 m/s, and the LED module was horizontally placed in the test section. The vapor chamber reduced the substrate surface temperature of LED module for 7–15%. Moreover, it presented significantly smaller thermal resistance than that of copper plate, i.e., a reduction of 19–29% in thermal resistance. The phase change heat transfer in vapor chamber contributed to much better heat transfer performance than the heat conduction in copper plate. A large amount of heat generated by LEDs was carried away quickly from the LED chips to the evaporator. Via the evaporation and condensation process, the heat was then transferred fast from the central area of evaporator to all the surface of the condenser, and finally dissipated by the heat sink with the fan. Besides, the separated vapor and liquid flow passages in the porous wicks with

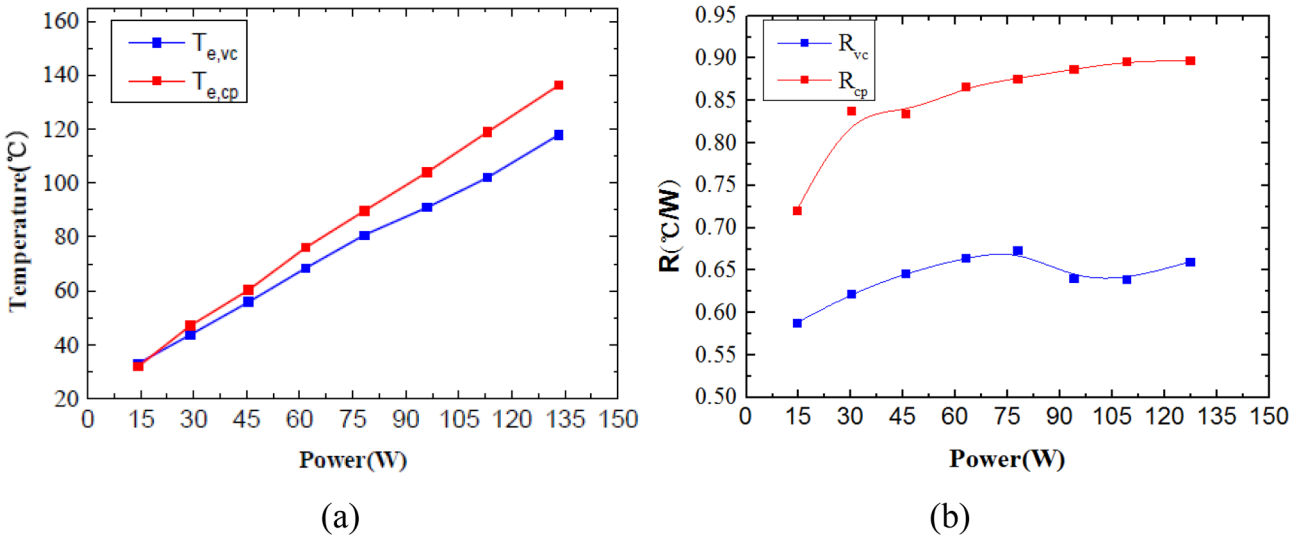

Fig. 8. Thermal performance of vapor chamber and copper plate at different input power of LED module: (a) Substrate surface temperature of LED module; (b) Thermal resistance.

radial reentrant microchannels reduced the shear force between the vapor and liquid counterflow, and enhanced the radial heat transport process. The unique wick structure of vapor chamber reduced the spreading resistance considerably. Therefore, much better heat dissipation performance can be reached by vapor chambers for LEDs.

When the input power of LEDs increased, it is clear that the substrate surface temperature of LED module of both vapor chamber and copper plate increased linearly, as can be seen in Fig. 8(a). The larger input power produced more heat flux in the LED module, and resulted in higher equilibrium temperature on the substrate surface. The thermal resistance of copper plate tended to increase monotonically. On the other hand, the thermal resistance of vapor chamber firstly increases with the increase of input power at low input power of LEDs, reached a plateau at about 78 W, and then tended to decline. The above trend can be explained as follows. As shown in Fig. 6(b), the LEDs heating sources were located in the middle of vapor chamber surface. As pointed out by Yang et al. [41] and Yang et al. [42], two effects contribute significantly to the overall thermal resistance of vapor chamer: (1) the vapor-liquid flow resistance in the height direction of vapor chamber; (2) the spreading resistance in the lateral (radial) direction of vapor chamber, i.e., from the center circular cavity to the edge of wick. At small to moderate heat input before 75 W, the spreading resistance effect predominated, as the evaporation mainly occurred in the center circular cavity of the evaporator wick, and most of the condensed liquid from the condenser return back from the edge to the center circular cavity. The spreading resistance increased with increasing heating input by the LEDs [42], thus induced a slight increase in the overall thermal resistance of VC. When the heating power increased to be larger than 75 W, the evaporation may emerge in all parts of the evaporator wick, including the edge areas of the evaporator wick. The vapor-liquid flow resistance played the dominant role in the overall thermal resistance of VC. The liquid layer thickness tended to decrease with the increase in the heating power, thus inducing a smaller vapor-liquid flow resistance [43]. The overall thermal resistance of VC thus tended to decrease. The above thermal resistance trend of VC is also in line with the findings of Ouhadou et al. [44] and Liu et al. [45].

4.2.2. Thermal performance at different air flow rates

The substrate surface temperature of LED module and thermal resistance of both heat sinks are shown in Fig. 9(a) and (b) at different air flow rates, respectively. The input power of LED module was 135 W, and the LED module was horizontally placed in the test section. The vapor chamber presented much smaller substrate surface temperature and thermal resistance than the copper plate. The substrate surface temperature decreased for 10–23%, and the thermal resistance decreased for 34–45% for the LED module with vapor chamber. This again demonstrated the superiority of vapor chamber in the thermal management of high-power LEDs.

From Fig. 9, it is also clear that both the substrate surface temperature of LED module and thermal resistance showed a decreasing trend with increasing air flow rates, which is true for both vapor chamber and copper plate. Higher air flow rate enhanced heat dissipation rate and cooling capacity, and thus induced lower substrate surface temperatures of the LED module and smaller thermal resistance. It should be noted that when air flow rate increased from 1 m/s to 3 m/s, it induced a rapid decrease in surface temperature and thermal resistance. Nevertheless, when the air flow rate exceeded 3 m/s, the substrate surface temperature and thermal resistance tend to decrease slightly or keep almost unchanged, and no notable variation can be seen. It means that when the air flow rate increased to 3 m/s, it may be sufficient to meet the heat dissipation demand for the LED module with the current heat flux. After that, the cooling effect was not significantly improved. As higher air flow rate needs extra energy and higher noise, the air flow rate should operate in within its recommended range during the thermal design of LED module.

4.2.3. Effect of inclination angles on thermal performance

For the utilization of high-power LEDs in different locations, the LED tests were conducted with the inclination angles within the range from 0° to 90°. The input power was 135 W and the air flow rate was 3 m/s. Fig. 10(a) and (b) shows the substrate surface temperature of LED module and thermal resistances of the vapor chamber and copper plate in different inclination angles. Once again, the vapor chamber showed much smaller substrate surface temperature and thermal resistance than the copper plate heat sink. The vapor chamber reduced thermal resistance for above 40%, i.e., 40–48%, and reduced the substrate surface temperature for 19–27% in all the inclination angles cases. Therefore, the vapor chamber enhanced the heat dissipation capacity regardless of the installation inclination angles.

From Fig. 10, with the increase in the inclination angles, the copper plate presented a larger magnitude of fluctuation in evaporator surface temperature and thermal resistance than the vapor chamber. Without the two-phase evaporation and condensation, the copper plate surface temperatures tended to change with increasing inclination angles, as the air flow and heat dissipation rates of fan cooling was dependent on the gravity considerably. On the other hand, for the vapor chamber, both thermal resistance and substrate surface temperature fluctuated within a small magnitude, i.e., the maximum variation of thermal

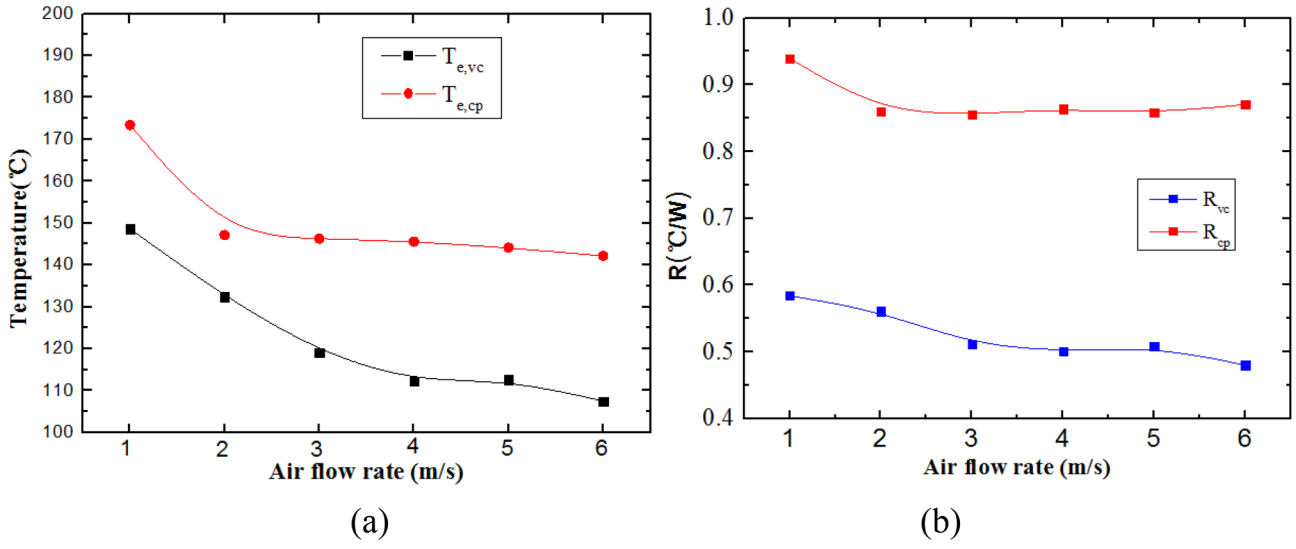

Fig. 9. Thermal performance of vapor chamber and copper plate at different air flow rates: (a) Substrate surface temperature of LED module; (b) Thermal resistance.

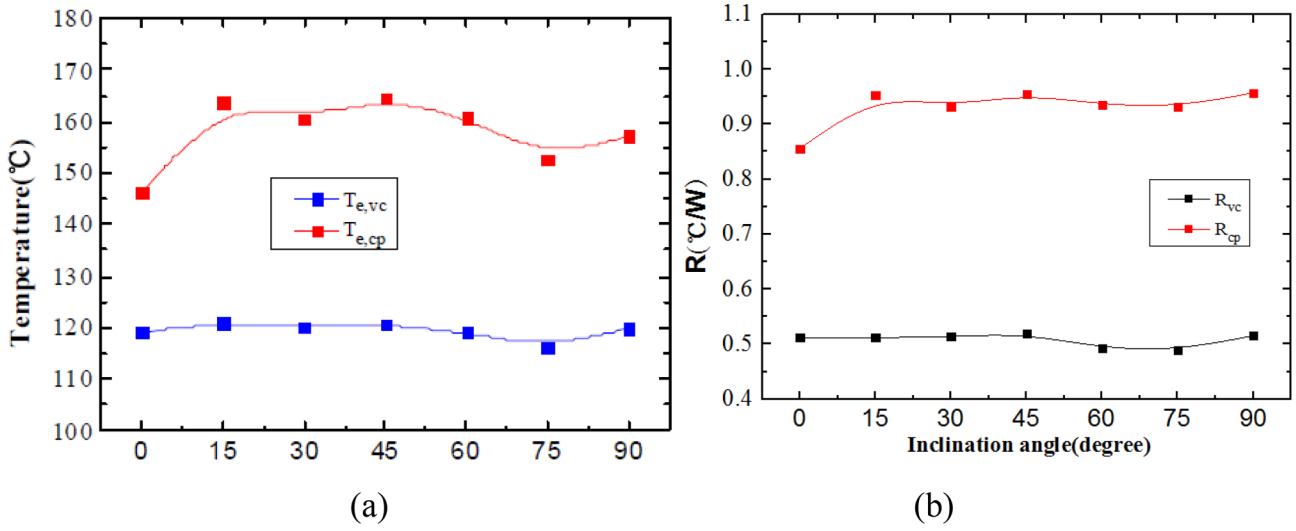

Fig. 10. Thermal performance of vapor chamber and copper plate at different inclination angles: (a) Substrate surface temperature of LED module; (b) Thermal resistance.

resistance was 0.024 ˚C/W, and the difference of substrate surface temperatures in different inclination angles was smaller than 5 ˚C. It indicates that the inclination angle had little effect on heat dissipation performance of the vapor chamber. This differed obviously from the common heat pipes [46], for which the heat pipe performance degrades considerably when the inclination angle increases, as the flow resistance of liquid from condenser to evaporator along common heat pipe increases remarkably. As aforementioned, the porous wicks in the evaporator featured many radial multi-artery reentrant mcirochannels. The large circular cavity in the Ω-shaped reentrant microchannels provided good passages for the fast liquid return. Besides, numerous tiny pores in the porous wick provided excellent capillary pressure, which also facilitated the flow back of working fluid from the condenser to evaporator. Therefore, even if in the anti-gravity conditions, the vapor chamber with radial multi-artery reentrant microchannels can sustain enough and fast liquid circulation, and maintained the continuous evaporation and condensation. Therefore, there is negligible effect of inclination angle for the vapor chamber. Such behavior is obviously favorable for the heat dissipation of LED module in practical titled installation conditions.

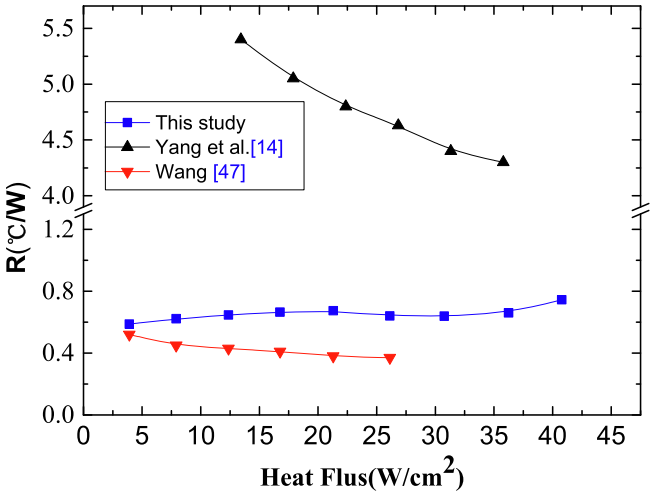

Fig. 11. Comparison of thermal resistance between the present vapor chamber and those reported in the literatures for heat dissipation of LED module.

4.2.4. Comparison with other studies

To evaluate thermal performance of the present LED module with vapor chamber further, the comparison between this study and other LED modules with VC in the literatures is conducted. Fig. 11 shows that the comparison results of thermal resistance performance of the LED module with VC between the current one and those reported in the literatures. Here the heat fluxes were utilized instead of the heat power to eliminate the area difference of LED chips.

Yang et al. [14] developed a polymer vapor chamber for cooling LED module. It consisted of a 1 mm thick copper frame, which was sandwiched between the top and bottom FR4 plates to form the vapor chamber. The VC was of an array of thermal via, formed by 0.5 mm holes drilled through the polymer, which were copper plated and filled with resin similar to the FR4 polymer. The distilled water was used as the working fluid. At the filling ratio of 36% which is similar to our study, the thermal resistance of vapor chamber was very large when the input power ranged within 6–16 W, i.e., 4.3–5.4 ˚C/W at input heat flux of 13.4–35.8 W/cm^2 of the LED module.

Wang [47] prepared a rectangular vapor chamber made of C1200 oxygen-free copper. Its dimensions were 90 × 90 × 3.0 mm^3, much larger than the present circular vapor chambers in this study. Pure water was chosen as the working fluid. The LED vapor chamber-based plate consisted of 4 × 4 LEDs, and the dimension LED chip was 1 × 1 mm^2. The heating power from the LEDs ranged within 1 W up to 6 W, much smaller than the present study. The thermal resistance was found to be 0.37–0.52 ˚C/W at input heat flux of 6.25–37.5 W/cm^2 of the LED module.

From Fig. 11, it can be noted that the present vapor chamber with radial multi-artery reentrant microchannels presented much smaller thermal resistance than the polymer VC in Yang et al. [14] for cooling LED module. This can be related to that the copper features much better thermal conductivity than polymer. Despite that the present vapor chamber featured a little larger thermal resistance than the rectangular vapor chamber in Wang [47], it can dissipated much larger input heat power of LED module than the one in Wang [47], which is especially promising in the application of high-power LEDs. Recognizing that ethanol presented much smaller latent of vaporization than water, it is expected that the present VC enhances thermal performance and shows competitive heat transfer performance if water is utilized instead of ethanol as the working liquid, as the same vapor chamber charged with water has been found to present much better thermal performance than charged with ethanol in previous reports [34,35]. Therefore, this vapor chamber with radial multi-artery reentrant microchannels seems to provide a promising alternative of efficient thermal management of

LED module.

5. Conclusion

A novel vapor chamber with radial multi-artery reentrant microchannels is developed for high-power LEDs. Thermal performance of LED module with this vapor chamber was tested by the comparison of a pure copper plate. The following conclusions can be summarized:

(1) The vapor chamber with radial multi-artery reentrant microchannels showed an earlier and faster increase in both evaporator and condenser surface temperatures than copper plate during the start-up process. The equilibrium state can be reached earlier than copper plate due to the phase change heat transfer in vapor chamber.
(2) The LED module with vapor chamber presented a 7–27% reduction in the substrate surface temperature against the copper plate one in all the test cases. Moreover, it reduced thermal resistance for 19–48%, indicating a much better thermal performance compared to the copper plate. The multi-artery reentrant microchannels provided separated vapor and liquid flow passages, and reduced the shear force between the vapor and liquid counterflow, and thus enhance the cooling capacity of vapor chamber.
(3) The substrate surface temperature of both vapor chamber and copper plate increased with increasing input power of LED module, and decreasing increasing air flow rate. The thermal resistance followed the same trend for copper plate. For vapor chamber, the thermal resistance decreased with increasing air flow rate, whereas it showed a non-monotonic behavior with increasing input power of LED module. When the air flow rate exceeded 3 m/s, no notable improvement in the thermal performance can be noted for both heat sinks. The air flow rate is suggested to be within 3 m/s during the thermal design of LED module with the present heat sinks.
(4) The inclination angle of LED module showed negligible effects on the thermal performance of vapor chamber, indicating that the present vapor chamber with radial multi-artery reentrant microchannels was able to maintain good thermal performance in the different installation conditions for practical applications.

Declaration of Competing Interest

The authors declare that they have no known competing financial interests or personal relationships that could have appeared to influence the work reported in this paper.

Acknowledgements

This research was financially supported under the Grants of the National Nature Science Foundation of China (No. 51775464), the Science and Technology Planning Project of Guangdong Province, China (No. 2017A010104002), the Science and Technology Planning Project for Industry-University-Research Cooperation in Huizhou City (Grant No. 2014B050013002), and is partially supported by Research Fund of Guangdong Key Laboratory of Precision Equipment and Manufacturing Technique (No. PEMT201903).

References

[1] X. Luo, R. Hu, S. Liu, K. Wang, Heat and fluid flow in high-power LED packaging and applications, Prog. Energy Combust. Sci. 56 (2016) 1–32.
[2] X. Ding, Y. Tang, Z. Li, Q. Chen, Y. Li, Y. He, Thermal and optical investigations of high power LEDs with metal embedded printed circuit boards, Int. Commun. Heat Mass Transf. 66 (2015) 32–39.
[3] Z. Lu, P. Bai, B. Huang, A. Henzen, R. Coehoorn, H. Liao, G. Zhou, Experimental investigation on the thermal performance of three-dimensional vapor chamber for LED automotive headlamps, Appl. Therm. Eng. 157 (2019).
[4] X.-J. Zhao, Y.-X. Cai, J. Wang, X.-H. Li, C. Zhang, Thermal model design and analysis of the high-power LED automotive headlight cooling device, Appl. Therm. Eng. 75 (2015) 248–258.
[5] M. Arik, J. Petroski, S. Weaver, Thermal challenges in the future generation solid state lighting applications: light emitting diodes, Proceedings of the IEEE Intersociety Conference on Thermal Phenomena Hawaii, 2002, pp. 113–120.
[6] J.-C. Shyu, K.-W. Hsu, K.-S. Yang, C.-C. Wang, Thermal characterization of shrouded plate fin array on an LED backlight panel, Appl. Therm. Eng. 31 (2011) 2909–2915.
[7] H. Ye, B. Li, H. Tang, J. Zhao, C. Yuan, G. Zhang, Design of vertical fin arrays with heat pipes used for high-power light-emitting diodes, Microelectron. Reliab. 54 (2014) 2448–2455.
[8] X. Zhang, R.-C. Li, Q. Zheng, Analysis and simulation of high-power LED array with microchannel heat sink, Adv. Manuf. 1 (2013) 191–195.
[9] X. Luo, W. Chen, R. Sun, S. Liu, Experimental and numerical investigation of a microjet-based cooling system for high power LEDs, Heat Transf. Eng. 29 (2008) 774–781.
[10] M. Wang, W. Cui, Y. Hou, Thermal spreading resistance of grooved vapor chamber heat spreader, Appl. Therm. Eng. 153 (2019) 361–368.
[11] G. Chen, Y. Tang, L. Duan, H. Tang, G. Zhong, Z. Wan, S. Zhang, T. Fu, Thermal performance enhancement of micro-grooved aluminum flat plate heat pipes applied in solar collectors, Renew. Energy 146 (2020) 2234–2242.
[12] H.S. Huang, Y.C. Chiang, C.K. Huang, S.L. Chen, Experimental investigation of flat heat pipe module applied to high-power light-emitting diodes, Exp. Heat Transf. 22 (2009) 26–38.
[13] J.-C. Wang, R.-T. Wang, T.-L. Chang, D.-S. Hwang, Development of 30Watt high-power LEDs flat heat pipe-based plate, Int. J. Heat Mass Transf. 53 (2010) 3990–4001.
[14] K.-S. Yang, T.-Y. Yang, C.-W. Tu, C.-T. Yeh, M.-T. Lee, A novel flat polymer heat pipe with thermal via for cooling electronic devices, Energy Convers. Manage. 100 (2015) 37–44.
[15] Y. Tang, L. Lin, S. Zhang, J. Zeng, K. Tang, G. Chen, W. Yuan, Thermal management of high-power LEDs based on integrated heat sink with flat heat pipe, Energy Convers. Manage. 151 (2017) 1–10.
[16] Y. Tang, D. Yuan, L. Lu, Z. Wang, A multi-artery flat heat pipe and its performance, Appl. Therm. Eng. 60 (2013) 15–23.
[17] D. Deng, Y. Tang, J. Zeng, S. Yang, H. Shao, Characterization of capillary rise dynamics in parallel micro V-grooves, Int. J. Heat Mass Transf. 77 (2014) 311–320.
[18] G. Franchi, X. Huang, Development of composite wicks for heat pipe performance enhancement, Heat Transf. Eng. 29 (2008) 873–884.
[19] F. Lefèvre, J.-B. Conrardy, M. Raynaud, J. Bonjour, Experimental investigations of flat plate heat pipes with screen meshes or grooves covered with screen meshes as capillary structure, Appl. Therm. Eng. 37 (2012) 95–102.
[20] J.C. Hsieh, H.J. Huang, S.C. Shen, Experimental study of microrectangular groove structure covered with multi mesh layers on performance of flat plate heat pipe for LED lighting module, Microelectron. Reliab. 52 (2012) 1071–1079.
[21] C. Oshman, Q. Li, L.-A. Liew, R. Yang, Y.C. Lee, V.M. Bright, D.J. Sharar, N.R. Jankowski, B.C. Morgan, Thermal performance of a flat polymer heat pipe heat spreader under high acceleration, J. Micromech. Microeng. 22 (2012).
[22] J. Wang, I. Catton, Enhanced evaporation heat transfer in triangular grooves covered with a thin fine porous layer, Appl. Therm. Eng. 21 (2001) 1721–1737.
[23] Y. Tang, D. Deng, L. Lu, M. Pan, Q. Wang, Experimental investigation on capillary force of composite wick structure by IR thermal imaging camera, Exp. Therm Fluid Sci. 34 (2010) 190–196.
[24] D. Deng, Y. Tang, G. Huang, L. Lu, D. Yuan, Characterization of capillary performance of composite wicks for two-phase heat transfer devices, Int. J. Heat Mass Transf. 56 (2013) 283–293.
[25] Y. Tang, D. Deng, G. Huang, Z. Wan, L. Lu, Effect of fabrication parameters on capillary performance of composite wicks for two-phase heat transfer devices, Energy Convers. Manage. 66 (2013) 66–76.
[26] Y. Li, H. He, Z. Zeng, Evaporation and condensation heat transfer in a heat pipe with a sintered-grooved composite wick, Appl. Therm. Eng. 50 (2013) 342–351.
[27] L. Jiang, H. Yong, Y. Tang, Y. Li, W. Zhou, L. Jiang, J. Gao, Fabrication and thermal performance of porous crack composite wick flattened heat pipe, Appl. Therm. Eng. 66 (2014) 140–147.
[28] G.S. Hwang, E. Fleming, B. Carne, S. Sharratt, Y. Nam, P. Dussinger, Y.S. Ju, M. Kaviany, Multi-artery heat-pipe spreader: lateral liquid supply, Int. J. Heat Mass Transf. 54 (2011) 2334–2340.
[29] Y.S. Ju, M. Kaviany, Y. Nam, S. Sharratt, G.S. Hwang, I. Catton, E. Fleming, P. Dussinger, Planar flat heat pipe with hybrid evaporator wicks for the thermal management of high-heat-flux and high-power optoelectronic devices, Int. J. Heat Mass Transf. 60 (2013) 163–169.
[30] D. Deng, Q. Huang, Y. Xie, X. Huang, X. Chu, Thermal performance of composite porous flat heat pipes with uniform radial grooves, Appl. Therm. Eng. 125 (2017) 1334–1344.
[31] A.E. Bergles, ExHFT for fourth generation heat transfer technology, Exp. Therm. Fluid Sci. 26 (2002) 335–344.
[32] Y. Chen, C. Zhang, M. Shi, J. Wu, G.P. Peterson, Study on flow and heat transfer characteristics of heat pipe with axial "Ω"-shaped microgrooves, Int. J. Heat Mass Transf. 52 (2009) 636–643.
[33] D. Deng, W. Wan, Y. Tang, Z. Wan, T. Zeng, D. Liang, Experimental investigations on flow boiling performance of reentrant and rectangular microchannels – a comparative study, Int. J. Heat Mass Transf. 82 (2015) 435–446.
[34] Y. Peng, W. Liu, B. Liu, J. Liu, K. Huang, L. Wang, W. Chen, The performance of the novel vapor chamber based on the leaf vein system, Int. J. Heat Mass Transf. 86 (2015) 656–666.
[35] X. Ji, J. Xu, A.M. Abanda, Copper foam based flat heat pipe for high heat flux dissipation, Exp. Thermal Fluid Sci. 40 (2012) 93–102.

[36] I. Kim, S. Cho, D. Jung, C.R. Lee, D. Kim, B.J. Baek, Thermal analysis of high power LEDs on the MCPCB, J. Mech. Sci. Technol. 27 (2013) 1493–1499.
[37] Y. Wang, J. Cen, F. Jiang, W. Cao, Heat dissipation of high-power light emitting diode chip on board by a novel flat plate heat pipe, Appl. Therm. Eng. 123 (2017) 19–28.
[38] J.P. Holman, Experimental Methods for Engineers, 8th ed., The McGrawHill Companies, 2012.
[39] Y. Luo, G. Liu, L. Zou, B. Yu, X. Wang, Thermal behavior investigation of silicon-Pyrex micro heat pipe, AIP Adv. 4 (3) (2014).
[40] Y. Li, Z. Li, W. Zhou, Z. Zeng, Y. Yan, B. Li, Experimental investigation of vapor chambers with different wick structures at various parameters, Exp. Therm Fluid Sci. 77 (2016) 132–143.
[41] C.T. Yang, W.C. Liu, C.Y. Liu, Measurement of thermal resistance of first-level Cu substrate used in high-power multi-chips LED package, Microelectron. Reliab. 52 (2012) 855–860.
[42] K. Yang, C. Chung, C. Tu, C. Wong, T. Yang, M.T. Lee, Thermal spreading resistance characteristics of a high power light emitting diode module, Appl. Therm. Eng. 70 (2014) 361–368.
[43] W. Liu, J. Gou, Y. Luo, M. Zhang, The experimental investigation of a vapor chamber with compound columns under the influence of gravity, Appl. Therm. Eng. 140 (2018) 131–138.
[44] M. Ouhadou, A.E. Amrani, C. Messaoudi, S. Zianic, Experimental investigation on thermal performances of SMD LEDs light bar: Junction-to-case thermal resistance and junction temperature estimation, Optik 182 (2019) 580–586.
[45] W. Liu, Y. Peng, T. Luo, Y. Luo, K. Huang, The performance of the flat heat pipe based on the plant leaf, Int. J. Heat Mass Transf. 98 (2016) 746–757.
[46] M. Mahdavi, S. Tiari, S. De Schampheleire, S. Qiu, Experimental study of the thermal characteristics of a heat pipe, Exp. Therm Fluid Sci. 93 (2018) 292–304.
[47] J.C. Wang, Thermal investigations on LED flat heat pipe based plates, Int. Commun. Heat Mass Transf. 38 (2011) 1206–1212.